

Electrochemical sensors based on porous nanocomposite films with weak polyelectrolyte-stabilized gold nanoparticles†

Sungwoo Kim,^a Younghoon Kim,^b Yongmin Ko^a and Jinhan Cho^{*b}

Received 7th February 2011, Accepted 25th March 2011

DOI: 10.1039/c1jm10560d

Porous hybrid multilayer films composed of cationic poly(allylamine hydrochloride) (PAH)- and anionic poly(acrylic acid) (PAA)-stabilized gold nanoparticles (Au_{NPs}) (*i.e.*, PAH-Au_{NPs} and PAA-Au_{NPs}) were prepared on indium tin oxide (ITO) electrodes using pH-controlled layer-by-layer (LbL) assembly method with subsequent acid treatment. The exponential growth of Au_{NP} deposition layers was caused by the “in-and-out” diffusion of PAH and PAA chains not bound to Au_{NPs}. Immersion of the films in an acidic solution (pH 2.4) converted the nonporous films to porous films *via* the disruption of ionic bonds and the rearrangement of free PE chains. In this case, the pH-induced porous films showed high electrochemical activity. Nonporous/dense films were found to prevent direct contact between probe molecules in solution and the catalytic components immobilized on an electrode. Electrodes coated with porous films, however, exhibited higher electrocatalytic activity toward nitric oxide oxidation compared with electrodes coated with nonporous films, despite the same levels of Au_{NP} loading. This work demonstrates that structural transformations *via* a facile pH treatment can significantly improve electrode sensitivity without the aid of porous supports or additional catalytic components.

Introduction

Metal nanoparticles have attracted considerable attention due to their unique optical, electrical, and catalytic properties. Gold nanoparticles (Au_{NP}) in particular are one of the most widely used metal nanoparticles for the preparation of electrochemical or biological devices.¹ For example, nanometre-sized gold nanoparticles display excellent catalytic behavior due to their relatively high surface area-to-volume ratio and their reactive interface properties, which differ notably from their bulk form.^{1b,2} However, the effective use of nanoparticles in devices, such as electrochemical sensors, requires that they are immobilized and well-dispersed throughout the film matrix. The preparation of nanocomposite films with a high density of catalytic Au_{NPs} may improve the electrocatalytic properties of the electrode. Other uses of Au_{NPs} involve their adsorption onto porous templates or the use of porous Au_{NPs} to increase the reactive surface areas of a catalyst. Zhou *et al.* reported that high sensitivity of glucose electrochemical biosensing could be achieved by depositing Au_{NPs} onto porous template nanotube supports.³

Porous gold particles with large surface areas may also be formed by etching the silica from a silica–gold nanocomposite.⁴ Recently, relatively thick electrocatalytic membrane films have been prepared for use in the fabrication of devices, such as fuel cells.⁵ A variety of factors, such as the loading level, reactive surface area of the metal catalysts, facile control of film thickness, and ease of manufacturing must be considered for the preparation of electrochemically active films.

Layer-by-Layer (LbL) assembly methods may be tuned to prepare a diversity of nanocomposite hybrid films with electrochemical properties. An important advantage of this method is that it enables the preparation of films with tailored film thickness, composition, and functionality on substrates of different size and shape.⁶ Additionally, various hydrophilic materials, from organic components to metal nanoparticles, can be embedded within LbL films and stabilized through, for example, electrostatic, hydrogen-bonding, or covalent interactions. Aimin *et al.* reported that highly efficient electrochemical sensors could be prepared from polyelectrolyte (PE)/Au_{NP} hybrid films by embedding 4-(dimethylamino)pyridine (DMAP)-stabilized Au_{NPs} in PE multilayers pre-assembled on indium tin oxide (ITO) electrodes.^{1b} LbL assembly is advantageous for the fabrication of highly porous thick film templates. For example, Rubner *et al.* reported that weak PE multilayers (*i.e.*, PE with a pH-dependent charge density) that adsorb large quantities of PE chains under specific pH conditions may be converted into porous films by acid treatment.⁷ Specifically, multilayers

^aSchool of Advanced Materials Engineering, Kookmin University, Jeongneung-dong, Seongbuk-gu, Seoul, 136-702, Korea

^bDepartment of Chemical and Biological Engineering, Korea University, Anam-dong, Seongbuk-gu, Seoul, 136-701, Korea. E-mail: jinhan71@korea.ac.kr; Fax: +82 2 926 6102; Tel: +82 2 3290 4852

† Electronic supplementary information (ESI) available: See DOI: 10.1039/c1jm10560d

composed of poly(allylamine hydrochloride) (PAH) with cationic amine groups ($-\text{NH}_3^+$) and poly(acrylic acid) (PAA) with anionic carboxylic acid groups ($-\text{COO}^-$), which deposit to form thick films at pH 7.5 for PAH and pH 3.5 for PAA, are highly porous after exposure to acidic conditions ($\text{pH} \leq 2.5$) due to the dissociation of electrostatic bonds and the rearrangement of the PE chains. As another example, Caruso *et al.* reported that porous PAH/PAA films could be obtained by exposing multilayers initially prepared from salt-containing PE solutions to pure water.⁸

Here, we report the preparation of highly sensitive electrochemical sensors composed of porous multilayers containing weak PE-encapsulated Au_{NPs} . Our motivation was to use the porous nanocomposite films containing Au_{NP} to increase the contact area between the probe materials and the catalytic Au_{NPs} to enhance the electrochemical properties. For this study, cationic and anionic Au_{NPs} were synthesized directly in, respectively, PAH and PAA aqueous solution (*i.e.*, PAH- Au_{NPs} and PAA- Au_{NPs}). The amine groups of PAH and the carboxylic acid groups of PAA had a high affinity toward and effectively stabilized the Au_{NPs} . As a result, the quantity of PE-encapsulated nanoparticles weakly adsorbed onto the substrate could be significantly enhanced by optimizing the solution pH, as in the case of pure weak PEs. Although Dotzauer *et al.* reported that catalytic membranes could be prepared from the LbL adsorption of PEs and Au_{NPs} within porous alumina supports,⁹ our approach differs wholly from previous approaches in that the highly sensitive sensors were obtained from pH-induced porous multilayers composed of PAH- Au_{NPs} and PAA- Au_{NPs} without the aid of porous supports. That is, porous nanocomposite films prepared *via* pH treatment displayed significantly higher electrocatalytic activity toward the oxidation of nitric oxide (NO) as well as increased electronic transfer between electrode and probe components (*i.e.*, $\text{Fe}(\text{CN})_6^{3-}$ and $\text{Fe}(\text{CN})_6^{4-}$) than was observed for nonporous films despite identical loading levels of the catalytic nanoparticles. pH-controlled LbL assembly based on weak PE-stabilized metal catalysts is advantageous for the preparation of a variety of electrocatalytic membranes that require high performance thick films with speedy manufacturing.

Experimental

Materials

Cationic poly(allylamine hydrochloride) (PAH) ($M_w = 70\,000$), anionic poly(acrylic acid) (PAA) ($M_w = 70\,000$) and gold precursor ($\text{HAuCl}_4 \cdot 3\text{H}_2\text{O}$) were purchased from Aldrich. PAH-encapsulated Au nanoparticles (PAH- Au_{NP}) were synthesized as follows: 0.85 mM $\text{HAuCl}_4 \cdot 3\text{H}_2\text{O}$ (33.4 mg) in 100 mL of a 1 mg mL^{-1} PAH aqueous solution were maintained at room temperature with vigorous stirring. The initial solution pH was adjusted to 9. In this case, the subsequent addition (2 mL) of 74 mM NaBH_4 resulted in a color change from pale yellow to red. The PAH- Au_{NP} solution was adjusted to pH 7.5 by addition of 0.1 M NaOH. The quantity of excess PAH chains not bound to Au_{NPs} was measured to be 91 mg total (*i.e.*, 0.91 mg mL^{-1}) using the separation method described below. The diameters of PAH- Au_{NPs} were measured by TEM imaging and found to be 15 ± 3.4 nm (50 particles sampled). Similarly, PAA-encapsulated Au

nanoparticles (PAA- Au_{NP}), 18 ± 4.2 nm in diameter, were synthesized using 0.85 mM HAuCl_4 in 100 mL of a 1 mg mL^{-1} PAA aqueous solution with subsequent addition (1 mL) of 74 mM NaBH_4 . The PAA- Au_{NP} solution was adjusted to pH 3.5 by the addition of 0.1 M HCl.

Analysis of the quantity of PE bound and not bound to Au_{NPs}

PAH- and PAA- Au_{NP} powders were obtained by centrifugation at 13 000 rpm. After centrifugation, residual water containing excess PAH or PAA chains was removed, and deionized water was subsequently added to sediment the powder. The excess PE (*i.e.*, PAH or PAA) not bound to Au_{NPs} was removed by three centrifugation/washing cycles. The amount of PE bound to Au_{NPs} was measured by annealing the powder at temperatures up to 700 °C at a heating rate of 5 °C min^{-1} . After thermal treatment, the quantity of PAH and PAA that had thermally decomposed was 36% and 28%, respectively. The total mass of pure metallic Au_{NPs} formed upon exposure to the reducing agents was calculated to be 16.74 mg in 100 mL aqueous solution. Therefore, the amount of PAH and PAA bound to Au_{NPs} was, respectively, 9.4 and 6.5 mg in 100 mL solution. The excess PAH and PAA was measured to be, respectively, 91 and 92.75 mg.

Preparation of LbL multilayer films

Si substrates with anionic surfaces were prepared by heating at 65 °C for 5 s in a 5 : 1 : 1 vol% solution of water, hydrogen peroxide, and 29% ammonia (RCA solution). Gold electrode substrates, for use in quartz crystal microbalances (QCMs), were irradiated with intense UV light (254 nm) instead of applying the RCA solution treatment. (PAH- Au_{NP} /PAA- Au_{NP})_n multilayers were prepared by dipping the substrates for 10 min in a cationic PAH- Au_{NP} solution (pH 7.5), washing the substrates by dipping in a pH 7.5 solution for 1 min, then rewashing the substrates by dipping in a pH 3.5 solution for 1 min. Anionic PAA- Au_{NPs} (pH 3.5) were subsequently deposited onto the PAH- Au_{NP} -coated substrates using the adsorption and washing conditions described above. The substrates were then rewashed by dipping in a pH 7.5 solution for 1 min. These processes were repeated until the desired number of layers was deposited. Porous nanocomposite multilayers were prepared by exposing the (PAH- Au_{NP} /PAA- Au_{NP})_n multilayer films to an acidic solution (pH 2.3) for 1 min, followed by drying in a nitrogen stream.

Quartz crystal microbalance measurements

A QCM device (Model: QCM200, SRS) was used to investigate the mass of material deposited after each adsorption step. The resonance frequencies of the QCM electrodes were *ca.* 5 MHz. The mass of adsorbed PAH- Au_{NP} and PAA- Au_{NP} , Δm , could be calculated from the change in QCM frequency, ΔF , according to the Sauerbrey equation ΔF (Hz) = $-56.6 \times \Delta m_A$, where Δm_A is the mass change per quartz crystal unit area, in $\mu\text{g cm}^{-2}$.

Size of PE- Au_{NP} and surface morphology of multilayers

The size of the synthesized PE- Au_{NPs} was investigated by HR-TEM (model: JEM-3010, JEOL). The surface morphology of

(PAH-Au_{NP}/PAA-Au_{NP}) multilayers adsorbed onto Si substrates was measured by FE-SEM (model: JSM-7401F, JEOL).

Cyclic voltammetry measurements

The electrochemical activities of multilayers adsorbed onto QCM Au electrodes were investigated by cyclic voltammetry (CV) (model: compactstat, IVIUM). NO sensing was performed using NaNO₂ stock solutions. NaNO₂ can generate free NO according to the following reaction,¹⁰



Results and discussion

Amine and carboxylic acid groups may be used as stabilizing functionalities during the synthesis of Au_{NPs} due to their high affinity for gold.¹¹ Considering that the charge density of these groups is pH-dependent, as is characteristic of weak electrolytes, cationic PAH (containing amine groups) and anionic PAA (containing carboxylic acid groups) may be used to prepare Au_{NPs} with pH-dependent characteristics. As shown in Fig. 1, this approach yielded PAH-stabilized Au_{NPs} (*i.e.*, PAH-Au_{NPs}) with diameters of 15 nm and PAA-stabilized Au_{NPs} (*i.e.*, PAA-Au_{NPs}), 18 nm in diameter, in aqueous media. The peak maxima in the plasmon absorption spectra of PAH-Au_{NPs} and PAA-Au_{NPs} were 532 and 543 nm, respectively. Although the red shift in the absorption spectra may have arisen from a variety of factors, such as a smaller nanoparticle–nanoparticle distance, a change in the refractive index of the solvent medium, or a change in the particle size, the absorption shift observed for PAA-Au_{NPs} was due mainly to the increase in Au_{NP} size.^{2d,2e,12}

(PAH-Au_{NP}/PAA-Au_{NP})_{*n*} multilayers were prepared by depositing PAH-Au_{NP} and PAA-Au_{NP} solutions adjusted to pH

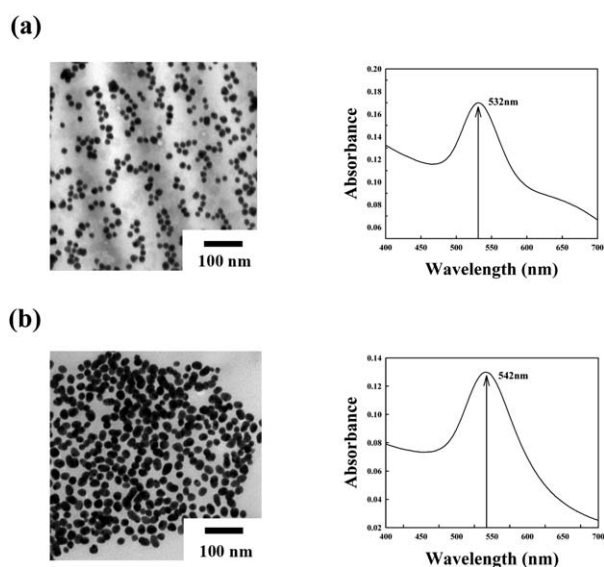


Fig. 1 TEM images and UV-visible spectra of (a) PAH-AuNPs and (b) PAA-AuNPs. The size of PAH-AuNPs and PAA-AuNPs were measured to be about 15 ± 3.4 and 18 ± 4.2 nm, respectively.

7.5 and 3.5, respectively. The PAH and PAA chains not bound to Au_{NPs} remained in the deposition solutions. The concentrations of excess PAH and PAA were measured to be about 0.91 and 0.94 mg mL⁻¹ in 100 mL deposition solution, and the percentages of PAH and PAA bound to Au_{NPs} were 9.4% and 6.5%, respectively (see the Experimental and ESI†, Fig. S1). The degree of ionization of PAH at pH 7.5 and PAA at pH 3.5 was measured to be about 80% and 7%, respectively.¹³ As shown in quartz crystal microbalance (QCM) data of Fig. 2, the build-up of (PAH-Au_{NP}/PAA-Au_{NP})_{*n*} multilayers followed a typical exponential growth pattern that could be explained by an “in-and-out diffusion” mechanism of excess PE chains during deposition (*i.e.*, polycations diffuse into the film during deposition, then out of the film during rinsing, and further out during polyanion deposition).¹⁴ This trend is very similar with QCM data shown in the build-up of (pH 7.5 PAH/pH 3.5 PAA)_{*n*} multilayers (see the ESI†, Fig. S2).

The quantities of adsorbed out-diffusing PEs and incoming oppositely charged PEs not bound to Au_{NPs} were proportional to the quantity of PE chains that diffused out of the film. Therefore, the amount of unbound or non-ionized PEs in coil, loop, or entangled structures within the multilayers significantly affected the exponential growth of the multilayers. PEs not bound to Au_{NPs} easily diffused out of the film surface. The plasmon absorption spectra of the Au_{NPs} showed an absorbance at 540 nm that increased linearly as the number of bilayers increased. No exponential growth or notable red shifts were observed. The same trend was observed in the linear increase in the adsorbed amounts during the electrostatic LbL assembly of

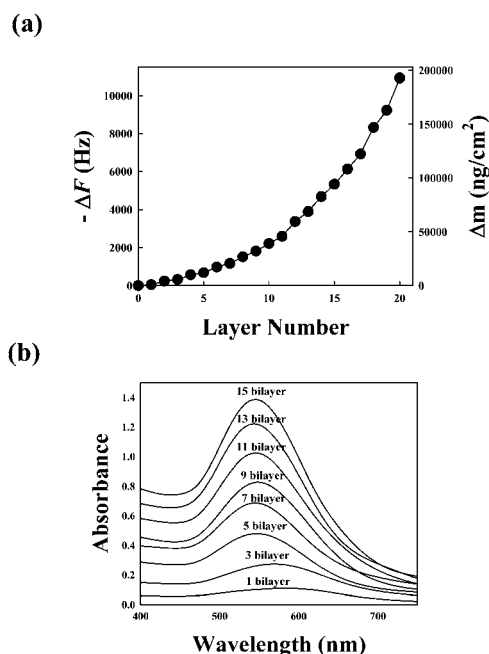


Fig. 2 (a) QCM data (*i.e.*, frequency and mass changes) of PAH-Au_{NP}/PAA-Au_{NP} multilayers as a function of layer number. The even and odd layer numbers in QCM data indicate PAA-Au_{NP} and PAH-Au_{NP}, respectively. (b) UV-visible spectra of PAH-Au_{NP}/PAA-Au_{NP} multilayers measured with increasing bilayer number.

PAH-Au_{NP}s and PAA-Au_{NP}s without excess PAH or PAA chains (see ESI†, Fig. S3).

Recently, Podsiadlo *et al.* reported that hybrid nanocomposite multilayers composed of weak PE and inorganic sheets (*i.e.*, (poly(ethyleneimine)/PAA/clay)_n) displayed exponential layer growth *via* fast diffusion/reptation of weak PEs through the openings between clay sheets, although the inserted clay sheet layers functioned as effective barriers for the diffusion of adsorbing PEs into the multilayers.^{14c} Therefore, it is reasonable to conclude that PAH and PAA chains not bound to Au_{NP} induced the exponential growth of PAH-Au_{NP}/PAA-Au_{NP} multilayers. Porous hybrid films were prepared by exposing (pH 7.5 PAH-Au_{NP}/pH 3.5 PAA-Au_{NP})₁₀ films to an acidic solution of pH 2.4, followed by washing with a pH 7 solution (Fig. 3). The film thickness increased from 370 to 410 nm, and the highly porous films formed after immersion in acidic solution mainly resulted from chain rearrangements and the phase separation associated with the partial breaking of ionic interchain pairs formed during the initial LbL assembly process. It was also reported by Mendelsohn *et al.* that pH 7.5 PAH/pH 3.5 PAA multilayer films are stable over extended immersion in water over a wide range of pH conditions from 3 ≤ pH ≤ 9, and however these films exposed to acidic water (pH ≤ 2.5) undergo

a significant structural change yielding interconnected porosity and film swelling.⁷ They also suggested that the pore volume in porous multilayer films is defined as 100[(H - H₀)/H], where H₀ and H are the film thickness before and after the pH transformation. Based on this definition, the pore volume in (PAH-Au_{NP}/PAA-Au_{NP})_n multilayers was calculated to be about 10%.

Pore formation was investigated in greater detail by measuring the electrochemical permeability of multilayer films using 10 mM Fe(CN)₆³⁻ and Fe(CN)₆⁴⁻ as probe components on ITO electrodes coated with (PAH-Au_{NP}/PAA-Au_{NP})_n multilayers in a pH 7.0 phosphate buffer solution (PBS) (Fig. 4a). Generally, K₃Fe[CN]₆/K₄Fe[CN]₆ undergoes reversible electrochemical reactions at a variety of electrodes.^{6e,15}

As the bilayer number (n) increased from 1 to 10, the peak current decreased and the peak separation (ΔE_p, the potential difference between the oxidation and reduction peak potentials, which is inversely proportional to the electron transfer rate) increased from 400 to 900 mV (*i.e.*, ΔE_p = 400 mV for n = 1, 535 mV for n = 3, 725 mV for n = 5, and 900 mV for n = 10). The electrode coated with 2-bilayered PAH/PAA multilayers without Au_{NP}s did not display a current response to K₃Fe[CN]₆/K₄Fe[CN]₆. Therefore, the nearly reversible electrochemical response observed in 5-bilayered PAH-Au_{NP}/PAA-Au_{NP} multilayers

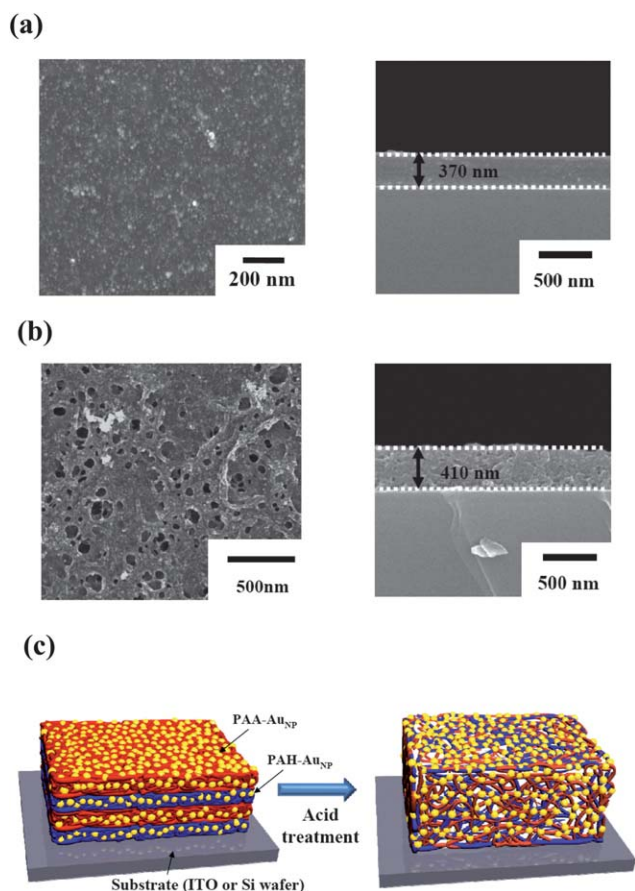


Fig. 3 (a) Top-view and cross-sectional SEM images of surface of (pH 7.5 PAH-Au_{NP}/pH 3.5 PAA-Au_{NP})₁₀ multilayer films (a) before and (b) after immersion in an aqueous bath of pH 2.4. (c) Schematics for structural change of PAH-Au_{NP}/PAA-Au_{NP} multilayers after acid treatment at pH 2.4.

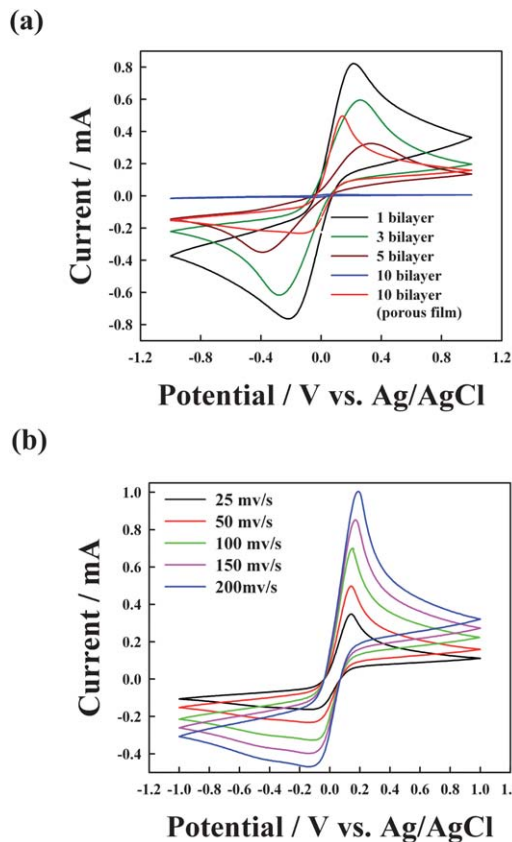


Fig. 4 (a) Cyclic voltammograms of 10 mM K₃Fe[CN]₆/K₄Fe[CN]₆ in pH 7.0 PBS at (a) (PAH-Au_{NP}/PAA-Au_{NP})_n = 1, 3, 5 and 10 multilayer-coated electrodes with scan rate of 50 mV S⁻¹ and (b) porous (PAH-Au_{NP}/PAA-Au_{NP})₁₀ film-coated electrodes as a function of scan rate. Porous films composed of 10 bilayers were prepared after immersion in an aqueous bath of pH 2.4.

indicated that Au_{NPs} in the multilayers improved the electron transfer between K₃Fe[CN]₆/K₄Fe[CN]₆ and the electrode. On the other hand, 10 bilayers did not display visible current responses for K₃Fe[CN]₆/K₄Fe[CN]₆ due to the poor electron transfer kinetics within the relatively thick PAH-Au_{NP}/PAA-Au_{NP} multilayers. The insulating PE chains not bound to Au_{NP} induced the exponential growth of multilayers with increasing bilayer number, *via* the in-and-out diffusion mechanism. Therefore, the thickly adsorbed PE chains effectively screened electron transfer between electrodes and probe components. However, exposure to acidic water at pH 2.4 increased the reversible anodic and cathodic currents significantly (55-fold and 25-fold increases for the cathodic and anodic currents, respectively), with a peak separation of 285 mV. Note that the redox properties were measured at a fixed scan rate of 50 mV S⁻¹. Increasing the scan rate results in higher intensity of redox peaks, as shown in Fig. 4b.¹⁶ Additionally, this reversible electrochemical response can be also observed in the electrode coated with porous (PAH/PAA)₁₀ multilayers without Au_{NPs} (see ESI†, Fig. S4).

Fig. 5 shows the electrochemical activity of PAH-Au_{NP}/PAA-Au_{NP} multilayers in pH 7.0 PBS as a function of bilayer number. In the potential region from 0 to 1.2 V, an oxidation peak was observed at 1.1 V and a reduction peak at 0.5 V. Bare ITO electrodes and PAH/PAA multilayer-coated electrodes displayed no current response within this potential region. Therefore, the redox peaks resulted from the oxidation and subsequent reduction of gold oxide (AuO_x) on the surfaces of Au_{NPs} as a result of positive potential polarization.^{16,15} Therefore, redox peak current intensities due to Au_{NPs} increased with increasing bilayer number (*i.e.*, the quantity of adsorbed gold nanoparticles increased). The redox currents of electrodes coated with porous multilayers, (PAH-Au_{NP}/PAA-Au_{NP})₁₀, were significantly higher than those of nonporous multilayer-coated electrodes despite having equal quantities of Au_{NPs}. These observations indicated that the chemical reversibility of the surface reactions on the Au_{NPs} was facilitated by the conversion from a nonporous structure with Au_{NPs} buried under the PE chains to a porous structure with a relatively large amount of externally exposed Au_{NPs}.

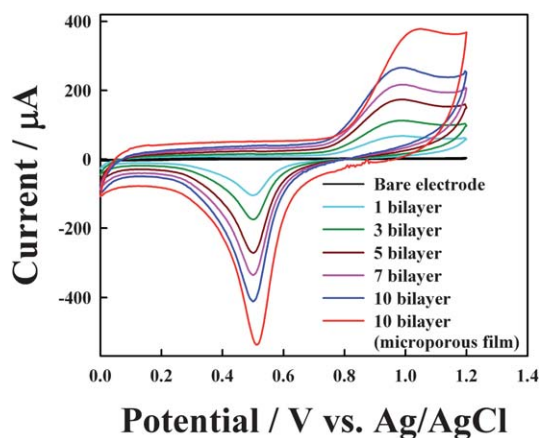


Fig. 5 Cyclic voltammograms of a bare ITO electrode and (PAH-Au_{NP}/PAA-Au_{NP})_n multilayer-modified electrodes in pH 7.0 PBS with scan rate of 50 mV S⁻¹. In this case, microporous films were prepared after immersion in an aqueous bath of pH 2.4.

NO synthesized by mammalian cells can act as a cytotoxic agent and may further react with oxygen to form a variety of reactive intermediates that are detrimental to the organic body.^{17,18} In solution, NO loses an electron to form NO⁺, and this process is aided by Au_{NPs}.^{16,19} The NO⁺ ion may then be further oxidized to form other more stable nitrogen products. Hybrid electrochemical sensors composed of porous (PAH-Au_{NP}/PAA-Au_{NP})₁₀ multilayers were designed for the detection and measurement of NO. Here, sodium nitrite (NaNO₂), which can generate free NO in acidic solution (pH < 4) was used as a precursor to measure the electrocatalytic activity of Au_{NPs} in the hybrid multilayers (see the Experimental). As shown in Fig. 6, the electrodes modified with Au_{NP}-based multilayers generated strong oxidation peaks around 1.23 V. The peak current increased with increasing NO concentration, implying that Au_{NPs} were catalytic toward the oxidation of NO. However, the electrodes coated with porous or nonporous PAH/PAA multilayer films without Au_{NPs} did not show such oxidation peak (see ESI†, Fig. S5).

The most important observation was that Au_{NP}-based multilayers with porous structures displayed higher electrocatalytic activity than nonporous multilayers at the same nitrite concentration. As mentioned above, the formation of porous structures that exposed large quantities of Au_{NPs} to the solution significantly increased the contact area between NO and the reactive

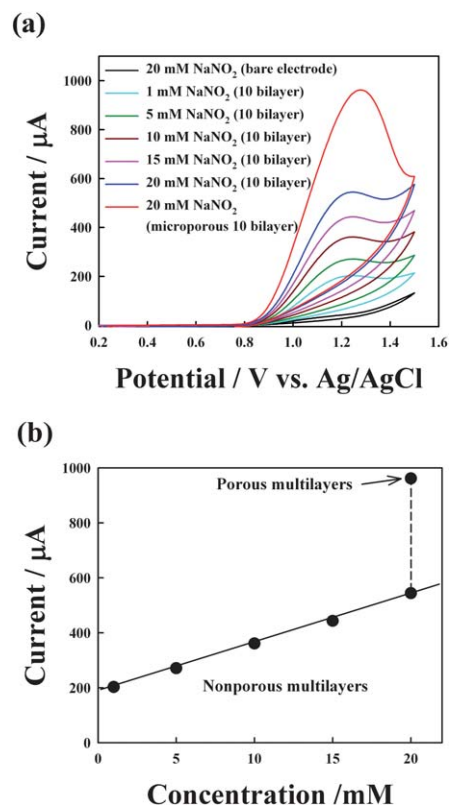


Fig. 6 (a) Cyclic voltammograms and (b) calibration curves of the amperometric responses of a bare ITO electrode and (PAH-Au_{NP}/PAA-Au_{NP})₁₀ multilayer-coated electrodes in pH 3.0 PBS containing 1, 5, 10, 15 and 20 mM NaNO₂ with scan rate of 50 mV S⁻¹. Porous film composed of 10 bilayers were prepared after immersion in an aqueous bath of pH 2.4.

Au_{NP} surfaces. As a result, the oxidation peak current corresponding to the electrochemical activity increased dramatically. These results suggest that electrochemical sensors based on catalytic metal nanoparticles can maximize electrochemical sensitivity through a facile structural transformation as well as the catalyst loading levels.

Conclusion

We have demonstrated that the electrochemical properties of PAH-Au_{NP}/PAA-Au_{NP} multilayers can be dramatically improved by the formation of pH-induced porous structures without increasing the Au_{NP} loading levels. The high electrochemical activities achieved in porous multilayers could be explained by the increased contact area between Au_{NPs} and the sensing components as well as the permeability of the sensing components into the multilayers. The exponential growth of deposited layers and the formation of porous structures after exposure to acidic solution resulted from the “in-and-out” diffusion of weak PE chains not bound to Au_{NPs}. A variety of catalytic nanoparticles, such as Pt, Pd, or TiO₂, in addition to Au, may be incorporated into PE multilayers using weak PE stabilizers. Therefore, our approach based on pH-induced porous hybrid multilayers provides a basis for the preparation of various catalytic membrane films requiring high performance and the fast manufacturing of layered nanocomposites.

Acknowledgements

This work was supported by National Research Foundation (NRF) grant funded by the Korea government (MEST) (2010-0029106; 2009-0085070; R11-2005-048-00000-0).

Notes and references

- (a) E. Hutter and J. H. Fendler, *Adv. Mater.*, 2004, **16**, 1685; (b) A. Yu, Z. Liang, J. Cho and F. Caruso, *Nano Lett.*, 2003, **3**, 1203; (c) D. Scott, M. Toney and M. Muzikár, *J. Am. Chem. Soc.*, 2008, **130**, 865; (d) Y. Xiao, F. Patolsky, E. Katz, J. F. Hanifield and I. Willner, *Science*, 2003, **299**, 1877; (e) J. Kim, S. W. Lee, P. T. Hammond and Y. Shao-Horn, *Chem. Mater.*, 2009, **21**, 2993; (f) W. B. Zhao, J. Park, A.-M. Caminade, S.-J. Jeong, Y. H. Jang, S. O. Kim, J.-P. Majoral, J. Cho and D. H. Kim, *J. Mater. Chem.*, 2009, **19**, 2006; (g) S.-H. Wu, C.-T. Tseng, Y.-S. Lin, C.-H. Lin, Y. Hung and C.-Y. Mou, *J. Mater. Chem.*, 2011, **21**, 789; (h) S. Song, Y. Qin, Y. He, Q. Huang, C. Fan and H.-Y. Chen, *Chem. Soc. Rev.*, 2010, **39**, 4234.
- (a) A. Henglein, *Chem. Rev.*, 1989, **89**, 1861; (b) L. Brus, *Appl. Phys. A: Solids Surf.*, 1991, **53**, 465; (c) A. N. Shipway, M. Lahav and I. Willner, *Adv. Mater.*, 2000, **12**, 993; (d) T. Teranishi, S. Hasegawa, T. Shimizu and M. Miyake, *Adv. Mater.*, 2001, **13**, 1699; (e) J. Cho and F. Caruso, *Chem. Mater.*, 2005, **17**, 4547.
- Y.-G. Zhou, S. Yang, Q.-Y. Qian and X.-H. Xia, *Electrochem. Commun.*, 2009, **11**, 216.
- A. Kumar, V. L. Pushparaj, S. Murugesan, G. Viswanathan, R. Nalamasu, R. J. Linhardt, O. Nalamasu and P. M. Ajayan, *Langmuir*, 2006, **22**, 8631.
- (a) W. Li, X. Wang, Z. Chen, M. Waje and Y. Yan, *Langmuir*, 2005, **21**, 9386; (b) D. C. Higgins, D. Meza and Z. Chen, *J. Phys. Chem. C*, 2010, **114**, 21982; (c) C. V. Rao and B. Viswanathan, *J. Phys. Chem. C*, 2010, **114**, 8661.
- (a) G. Decher, *Science*, 1997, **277**, 1232; (b) F. Caruso, R. A. Caruso and H. Möhwald, *Science*, 1998, **282**, 1111; (c) P. Podsiadlo, A. K. Kaushik, E. M. Arruda, B. S. Shim, J. D. Xu, H. Nandivada, B. G. Pumphlin, J. Lahann, A. Ramamoorthy and N. A. Kotov, *Science*, 2007, **318**, 80; (d) C. Jiang, S. Markutsya, Y. Pikus and V. V. Tsukruk, *Nat. Mater.*, 2004, **3**, 721; (e) S. Kim, J. Park and J. Cho, *Nanotechnology*, 2010, **21**, 375702; (f) Y. Kim, C. Lee, I. Shim, D. Wang and J. Cho, *Adv. Mater.*, 2010, **22**, 5140; (g) H. Kang, C. Lee, S. C. Yoon, C.-H. Cho, J. Cho and B. J. Kim, *Langmuir*, 2010, **26**, 17589; (h) B. Lee, Y. Kim, S. Lee, Y. S. Kim, D. Wang and J. Cho, *Angew. Chem., Int. Ed.*, 2010, **49**, 359.
- J. D. Mendelsohn, C. J. Barrett, V. V. Chan, A. J. Pal, A. M. Mayes and M. F. Rubner, *Langmuir*, 2000, **16**, 5017.
- A. Fery, B. Scholer, T. Cassagneau and F. Caruso, *Langmuir*, 2001, **17**, 3779.
- D. M. Dotzauer, J. Dai, L. Sun and M. L. Bruening, *Nano Lett.*, 2006, **6**, 2268.
- (a) G. Stedman, *Adv. Inorg. Chem. Radiochem.*, 1979, **22**, 113; (b) F. A. Cotton and G. Wilkinson, *Advanced Inorganic Chemistry*, 5th ed., Wiley, New York, 1988, p 327.
- (a) A. Kumar, S. Mandal, P. R. Selvakannan, P. Pasricha, A. B. Mandale and M. Sastry, *Langmuir*, 2003, **19**, 6277; (b) K. S. Mayya and F. Caruso, *Langmuir*, 2003, **19**, 6987; (c) H. Zhang and H. Cui, *Langmuir*, 2009, **25**, 2604.
- (a) S. Link, C. Burda, M. B. Mohamed, B. Nikoobakht and M. A. El-Sayed, *J. Phys. Chem. A*, 1999, **15**, 3256; (b) J. Schmitt, P. Mächtle, D. Eck, H. Möhwald and C. A. Helm, *Langmuir*, 1999, **15**, 3256.
- J. Choi and M. F. Rubner, *Macromolecules*, 2005, **38**, 116.
- (a) E. Hubsch, V. Ball, B. Senger, G. Decher, J.-C. Voegel and P. Schaaf, *Langmuir*, 2004, **20**, 1980; (b) C. Porcel, P. Lavalie, V. Ball, G. Decher, B. Senger, J.-C. Voegel and P. Schaaf, *Langmuir*, 2006, **22**, 4376; (c) P. Podsiadlo, M. Michel, J. Lee, E. Verploegen, N. W. S. Kam, V. Ball, J. Lee, Y. Qi, A. J. Hart, P. T. Hammond and N. A. Kotov, *Nano Lett.*, 2008, **8**, 1762.
- (a) J. J. Harris and M. L. Bruening, *Langmuir*, 2000, **16**, 2006; (b) V. Pardo-Yissar, E. Katz, O. Lioubashevski and I. Willner, *Langmuir*, 2001, **17**, 1110.
- (a) M. Li, M. Xu, N. Li, Z. Gu and X. Zhou, *J. Phys. Chem. B*, 2002, **106**, 4197; (b) B. A. Gregg and A. Heller, *Anal. Chem.*, 1990, **62**, 258; (c) J. Park, I. Kim, H. Shin, M. J. Lee, Y. S. Kim, J. Bang, F. Caruso and J. Cho, *Adv. Mater.*, 2008, **20**, 1843.
- (a) L. D. Burke, D. Bethell, C. J. Kiely and D. J. Schiffrin, *Langmuir*, 1996, **12**, 4723; (b) L. D. Burke and P. F. Nugent, *Gold Bull.*, 1998, **31**, 39.
- (a) D. A. Wink and J. B. Mitchell, *Free Radical Biol. Med.*, 1998, **25**, 434; (b) L. J. Ignarro, G. M. Bugga, K. S. Wood, R. E. Byrns and G. Chaudhuri, *Proc. Natl. Acad. Sci. U. S. A.*, 1987, **84**, 9265.
- (a) A. Ciszewski, G. Milczarek, E. Kubaszewski and M. Lozynski, *Electroanal.*, 1998, **10**, 628; (b) M. Zhu, M. Liu, G. Shi, F. Xu, X. Ye, J. Chen, L. Jin and J. Jin, *Anal. Chim. Acta*, 2002, **455**, 199.